

A Decoupled Spatio-Temporal Framework for Skeleton-based Action Segmentation

Yun-Heng Li, Zhong-Yu Li, Shanghua Gao, Qilong Wang, Qibin Hou, *Member, IEEE*,
Ming-Ming Cheng, *Senior Member, IEEE*

Abstract—Effectively modeling discriminative spatio-temporal information is essential for segmenting activities in long action sequences. However, we observe that existing methods are limited in weak spatio-temporal modeling capability due to two forms of decoupled modeling: (i) cascaded interaction couples spatial and temporal modeling, which over-smooths motion modeling over the long sequence, and (ii) joint-shared temporal modeling adopts shared weights to model each joint, ignoring the distinct motion patterns of different joints. In this paper, we present a **Decoupled Spatio-Temporal Framework (DeST)** to address the above issues. Firstly, we decouple the cascaded spatio-temporal interaction to avoid stacking multiple spatio-temporal blocks, while achieving sufficient spatio-temporal interaction. Specifically, DeST performs once unified spatial modeling and divides the spatial features into different groups of sub-features, which then adaptively interact with temporal features from different layers. Since the different sub-features contain distinct spatial semantics, the model could learn better interaction patterns at each layer. Meanwhile, inspired by the fact that different joints move at different speeds, we propose joint-decoupled temporal modeling, which employs independent trainable weights to capture distinctive temporal features of each joint. On four large-scale benchmarks of different scenes, DeST significantly outperforms current state-of-the-art methods with less computational complexity.

Index Terms—Skeleton-based action segmentation, decoupled spatio-temporal interaction, joint-decoupled temporal modeling

1 INTRODUCTION

TEMPORAL action segmentation (TAS), which aims at classifying each video frame, is critical for various practical applications, such as surveillance [1], [2], assisted rehabilitation [3], [4], interactive robotics [5], [6] and virtual reality [7], [8]. Current works on action segmentation can be divided into RGB video-based methods and skeleton-based methods. RGB video-based approaches adopt two stages to model spatial and temporal information, respectively, where high computational costs are required to capture the pixel-level appearance information. In contrast, skeleton-based action segmentation utilizes one stage for unified spatial and temporal modeling and is more efficient as the skeleton acquired by motion capture systems already represents motion information. Moreover, skeleton data is more robust to appearance variation and environmental noises, *e.g.*, scene and illumination changes [9], [10], [11]. Based on the skeleton data, previous works [12], [13], [14], [15], [16], [17], [18], [19] have achieved great progress in identifying short action clips.

Despite the remarkable progress, segmenting all actions in a long skeleton sequence is still extremely challenging. Existing temporal action segmentation methods [20], [21], [22], [23] generally employ spatial and temporal graph convolution networks (GCNs) to model the spatial and temporal dependencies among joints and perform spatio-temporal interaction to extract motion features, as illustrated in Fig. 1(a). However, we observe that these GCNs-based approaches are limited to weak spatio-temporal

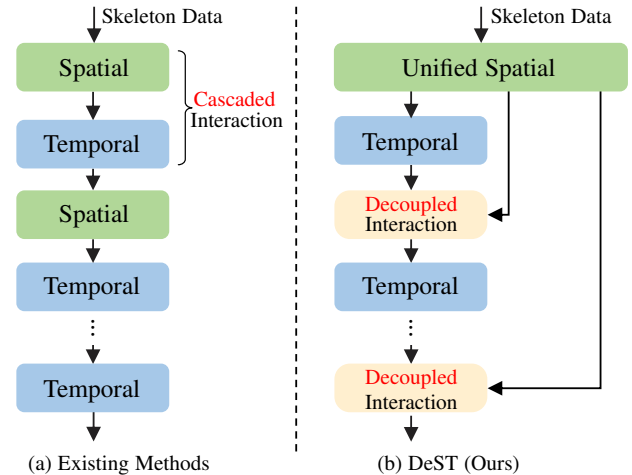


Fig. 1. Comparison of existing and our proposed methods for spatio-temporal modeling in the skeleton-based action segmentation. (a) Existing methods employ coupled spatial and temporal modeling for **cascaded** interaction. (b) In contrast, the proposed DeST **decouples** the cascaded spatial-temporal interaction by adopting unified spatial modeling to extract different groups of spatial sub-features, which adaptively interact with temporal features from different layers, respectively.

modeling capability for long skeleton sequences due to two forms of coupled modeling, *i.e.*, (i) cascaded interaction pattern and (ii) joint-shared temporal modeling. Specifically, identifying complex actions needs to extract discriminative spatio-temporal representations by interacting with spatial and temporal information of joints. Nevertheless, to perform multiple spatio-temporal interactions, the cascaded interaction methods alternately stack spatial and temporal modeling modules, which over-smooths the spatio-temporal information [24], [25] and leads to high computational costs [10], [11]. In addition, in previous temporal GCNs, joint-shared weights [20], [21] are used to model the

- Y.-H. Li, Z.-Y. Li, S. Gao, Q. Hou, and M.-M. Cheng are with VCIP, School of Computer Science, Nankai University, Tianjin 300350, China. E-mail: {yunhengli; lizhongyu}@mail.nankai.edu.cn (Corresponding author: Q. Hou)
- Q. Wang is with the College of Intelligence and Computing, Tianjin University, Tianjin 300350, China.
- This work was supported in part by the Supercomputing Center of Nankai University.
- Our code is available at: <https://github.com/lyhisme/DeST>.

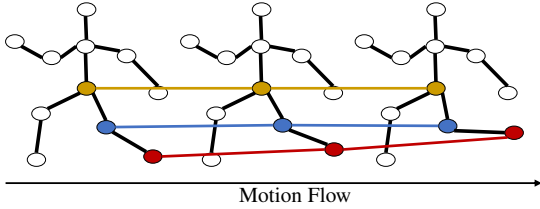


Fig. 2. Illustration of motion of body joints. The various joints exhibit distinct motion speeds.

temporal dependencies of all joints. However, this joint-shared strategy ignores the fact that different joints have different motion speeds. For instance, as shown in Fig. 2, when a person moves, the feet typically move faster than other joints, whereas the waist moves more slowly. Once joint-shared weights are trained on all joints, the dynamic temporal information of the foot is weakened, making it ambiguous to distinguish some actions, like “Running” and “Walking.” Thus, such joint-shared temporal modeling will lose information about joint motion differences, restricting the temporal modeling capability.

To address the limitations mentioned above, we propose a Decoupled Spatio-Temporal Framework (DeST), as illustrated in Fig. 1(b). Unlike existing methods [20], [21], [22], [23] (in Fig. 1(a)), DeST utilizes decoupled interaction (instead of cascaded interaction) to perform spatio-temporal modeling and adopts independent weights (not joint-shared weights) to model the temporal dependencies of each joint. Specifically, our DeST involves of two core components, including decoupled spatio-temporal interaction (DSTI) and joint-decoupled temporal modeling (JTM). To avoid the effect of over-smoothing brought by the coupled spatio-temporal modeling, DSTI decouples cascaded spatio-temporal interaction by adopting a single-layer unified spatial modeling and dividing the spatial features into different groups of spatial sub-features. Particularly, various spatial sub-features focus on distinct spatial semantics and adaptively interact with the temporal features from different layers, enabling learning better interaction patterns at different layers. As such, our DeST can capture richer spatio-temporal representations in long skeleton action sequences. To generate more effective temporal features, JTM adopts independent trainable weights to capture temporal dependencies for each joint separately. By adopting JTM, the learned temporal dependencies can be adapted to the unique motion attributes of each joint and hence improve the temporal modeling ability of the model.

To evaluate the effectiveness of our DeST method, experiments are conducted on four long-sequence skeleton-based TAS benchmarks with diverse scenes, including competitive sports (*e.g.*, MCFS-22 [26] and MCFS-130 [26] datasets), daily activities (*e.g.*, PKU-MMD [27] dataset), and typical warehousing activities (*e.g.*, LARa [28] dataset). Our DeST consistently achieves superior performance with lower computational costs.

Our contributions can be summarized as follows:

- In this paper, we propose a Decoupled Spatio-Temporal (DeST) framework, which to our best knowledge, makes the first attempt to decouple spatio-temporal modeling for effective skeleton-based action segmentation.
- We propose a decoupled spatio-temporal interaction module and a joint-decoupled temporal modeling module to decouple the cascaded spatio-temporal interaction and learn the discriminative motion pattern of each joint, respectively.

- Extensive experimental results demonstrate that our proposed DeST method achieves new state-of-the-art results with even lower model complexity than previous works.

2 RELATED WORK

2.1 RGB-based Temporal Action Segmentation

Most works follow a two-stage process, *i.e.*, feature extracting and temporal modeling, to segment RGB-based videos. The first stage simply uses pre-trained networks [29] to extract the spatial features of each video frame. Most action segmentation methods focus on the second stage to model temporal context information. Early approaches [30], [31] mostly adopt recurrent neural networks for temporal modeling. To capture long-range dependencies, temporal convolution networks are proposed for action segmentation, including encoder-decoder architecture [32], temporal series pyramid networks [33], and multi-layer dilated convolutions [34], [35]. Meanwhile, for these TCN-based methods, Gao et al. [36], [37] proposed a global-to-local search scheme to efficiently search for receptive field combinations. On the other hand, transformer-based models [38], [39], [40] are proposed for action segmentation. For example, Bahrami et al. [40] presented LTContext that leverages sparse attention to capture the long-term context and windowed attention to model the local information. However, the above methods still tend to over-segment actions. To address this problem, many researchers explore different approaches, *e.g.*, additional network branches [41], [42], two-step methods [33], or hierarchical refiner [43].

Recently, multi-modal learning [44] and diffusion models [45] have also been employed for action segmentation. However, these RGB-based methods require high-cost computational resources to extract motion representations by processing RGB images or temporal optical flow [46]. The generated motion representations also lose fine-grained information, especially joint connections [47]. In this work, we focus on another line of methods, *i.e.*, skeleton-based action segmentation. Compared to RGB-based methods, skeleton-based methods are more efficient and robust to the variations of the environment in that the human skeleton conveys high-level motion information.

2.2 Skeleton-based Temporal Action Segmentation

By using low-cost MoCap systems, the motion of the skeleton can be captured as a time series. Filtjens et al. [20] first proposed multi-stage spatio-temporal graph convolution neural networks (MS-GCN) by replacing the initial stage of temporal convolutions with spatio-temporal graph convolutions. On top of MS-GCN, Xu et al. [21] created a combined network by connectionist temporal classification loss. Moreover, Tian et al. [48] proposed spatio-temporal attention blocks to model spatial correlation and temporal correlation separately. However, these works utilize shared weights of temporal graph convolution or sliding window attention to model temporal dependencies, limiting the temporal learning capability. To enhance temporal semantics, Liu et al. [22] proposed spatial focus attention to model the spatial dependencies and multi-layer TCNs to model temporal dependencies. Similarly, Li et al. [23] proposed an involving distinguished temporal graph convolution network (IDT-GCN) to improve the capability to model spatial-temporal information and utilize extra information, *i.e.*, the order of action proceeding, to capture the segment-level encoding features and action boundary representations. Nevertheless, these GCN-based methods conduct

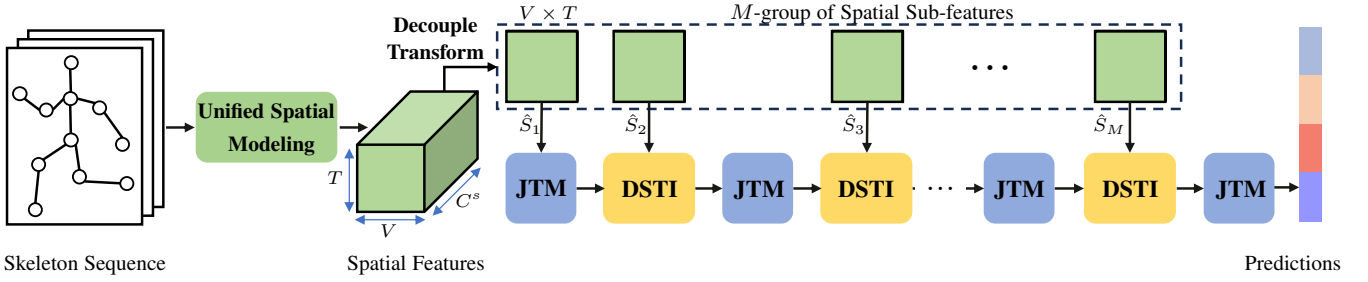


Fig. 3. Framework of the proposed end-to-end Decoupled Spatio-Temporal Framework (DeST). We first employ unified spatial modeling networks (introduced in Section 3.1) to capture spatial features $S \in \mathbb{R}^{C^s \times T \times V}$ of the joints, where C^s , T , and V denote the numbers of output channels, frames, and joints, respectively. Then, the obtained spatial features S are divided into a group of spatial sub-features $\hat{S}_i \in \mathbb{R}^{V \times T}$ that could learn different spatial semantics. Moreover, the JTM (introduced in Section 3.3) module is utilized to model the temporal dependencies of each joint individually, achieving discriminative temporal features. In the DSTI (introduced in Section 3.2) block, spatial sub-features adaptively interact with temporal features, capturing complex spatio-temporal representations.

single or multiple cascaded spatio-temporal interactions, which over-smooth the spatio-temporal features and fail to capture complex spatio-temporal information effectively. Unlike these methods, we propose a decoupled spatio-temporal architecture that adopts unified spatial modeling to extract spatial sub-features and let these sub-features interact with temporal features to avoid cascaded spatio-temporal interactions. Meanwhile, we utilize independent weights to capture distinct temporal dependencies of each joint, enhancing the temporal modeling capabilities.

2.3 Skeleton-based spatio-temporal Networks

The spatio-temporal graph convolution networks and transformers have also been widely used to model human action dynamics for other skeleton-based action understanding tasks, including short action recognition [49], [50], [51], [52], temporal action detection [53], [54], [55], [56], and human motion prediction [57], [58], [59], [60]. However, these methods are not suitable for segmenting actions in long sequences. On one hand, the problems of joint-shared temporal modeling and cascaded spatio-temporal interaction, which are demonstrated in Section 1, also exist in these tasks. For example, action recognition methods model the relations between body joints by alternately stacking spatial graph convolutions and temporal graph convolutions [61], [62], [63], [64], [65], [66], [67], [68], [69], thus over-smoothing spatio-temporal information and failing to identify multiple actions in long action sequences. Moreover, these tasks usually model spatial and temporal information in different domains. For instance, some human motion prediction approaches [60], [70], [71] separate spatio-temporal information into the spatial and temporal branches. Differently, the proposed DeST models the motion of joints by unified spatio-temporal modeling.

3 METHOD

Let $\mathcal{V} = \{\alpha_{vt} \mid v \in [1, V], t \in [1, T]\}$ be a skeleton sequence, where V and T denote the number of joints and the number of frames, respectively. Action segmentation aims to identify the category for each frame. In this section, we propose the Decoupled spatio-temporal model (DeST), an end-to-end framework for skeleton-based action segmentation. The overall architecture is shown in Fig. 3, which consists of two core components: 1) decoupled spatio-temporal interaction (DSTI) architecture to avoid the over-smoothing issue brought by the coupled spatio-temporal modeling and achieve sufficient spatio-temporal interaction and 2) joint-decoupled temporal modeling (JTM) module to enhance

TABLE 1
The definition and description of symbols.

Symbols	Dimensions/Type	Meaning
V	scalar	Number of joints.
T	scalar	Number of frames.
C, C^s, C^t	scalar	Number of Channel.
Multi-scale Spatial Modeling (MSM) in Section 3.1		
X	$C \times T \times V$	Joint features.
\hat{A}	$V \times V$	Normalized adjacency matrix.
$A^{(k)}$	$V \times V$	k -adjacency matrix.
$B^{(k)}$	$V \times V$	Learnable matrix.
Decoupled Spatio-Temporal Interaction (DSTI) in Section 3.2		
S	$C^s \times T \times V$	Spatial features output by spatial modeling.
S_i	$\frac{C^s}{M} \times T \times V$	Spatial sub-features.
\hat{S}_i	$V \times T$	Joint-level features transform from S_i .
R	$C^t \times T$	Spatio-temporal features output by STI.
M	scalar	Number of groups of the spatial sub-features.
Joint-wise Temporal Modeling (JTM) in Section 3.3		
J	$V \times T$	Input features for JTM.
$\mathcal{T}(J)$	$C^t \times T$	Temporal features output by JTM.

the discrimination of temporal features. For convenience, some important symbols and their definitions are listed in Tab. 1.

3.1 Preliminary

To make the paper understandable, we first briefly present unified spatial modeling for skeleton-based action segmentation.

Multi-scale spatial modeling. Recently, graph convolution networks have been successfully adopted to aggregate spatial information of joints [47], [60], [72], [73], [74], [75]. Inspired by MS-G3D [76], we adopt multi-scale spatial modeling to capture the spatial dependencies between joints. Specifically, we first define a k -adjacency matrix $A^{(k)} \in \mathbb{R}^{V \times V}$, which connects the joints at distance k , as follows:

$$A_{ij}^{(k)} = \begin{cases} 1, & \text{if } d(\alpha_i, \alpha_j) = k, \\ 1, & \text{if } i = j, \\ 0, & \text{otherwise,} \end{cases} \quad (1)$$

where $d(\alpha_i, \alpha_j)$ denotes the shortest distance (*i.e.*, the number of edges) between joints α_i and α_j . Given the C -dim features $X \in \mathbb{R}^{C \times T \times V}$ of V joints, through matrix multiplication, *i.e.*, $XA^{(k)}$, the dependencies between joints at the distance k are captured. In addition to the adjacency matrix $A^{(k)}$ defined

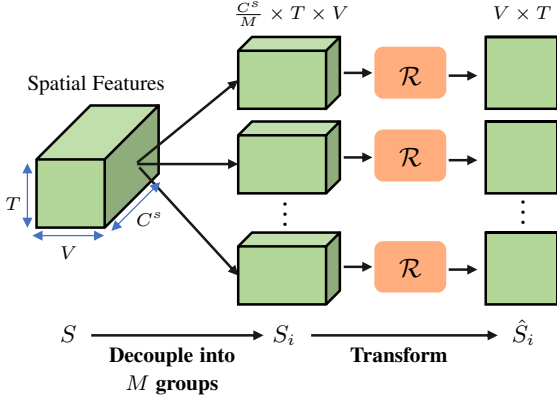


Fig. 4. Illustration of decoupling and transforming the spatial sub-features. The \mathcal{R} function, as defined in Section 3.2, transforms the spatial sub-features to align with the number of dimensions of temporal features. Then, in Section 3.2, the transformed spatial sub-features interact with temporal features from different layers.

by the physical connections of body joints, we construct a $V \times V$ adjacency matrix $B^{(k)}$ that is trainable and hence can adaptively learn the relationships between joints. Through combining the two adjacency matrices at different distances, the multi-scale spatial features $S \in \mathbb{R}^{C^s \times T \times V}$ can be aggregated as follows:

$$S = \text{MLP}(W^S X([\hat{A}^{(1)} + B^{(1)}] \parallel \dots \parallel [\hat{A}^{(K)} + B^{(K)}])), \quad (2)$$

where $\parallel \cdot \parallel$ is the concatenation operation along the second dimension, W^S is a weight tensor, and $\hat{A}^{(k)}$ is the normalized matrix¹ following [61], [76]. The MLP means a multilayer perceptron to adjust the number of channels. In particular, the aggregated spatial feature S encodes multi-scale spatial representations by adopting multiple adjacency matrices at distances from 1 to K . By default, K is set as 13 here.

3.2 Decoupled spatio-temporal Interaction

It is crucial to establish the spatio-temporal interaction in skeleton-based action segmentation. Following GCN-based methods [61], existing action segmentation methods [20], [21], [22], [23] perform cascaded spatio-temporal interaction by coupling the spatial and temporal modeling. However, we observe that 1) some methods [20], [21] stack multiple cascaded spatio-temporal modeling blocks, over-smoothing motion information and producing weak spatio-temporal features. 2) Other methods [22], [23] employ a single cascaded spatio-temporal interaction, resulting in an insufficient spatio-temporal interaction. To solve these problems, we propose a Decoupled Spatio-Temporal Interaction (DSTI) architecture to avoid cascaded interaction and achieve efficient spatio-temporal interaction, as shown in Fig. 3.

Decoupled spatio-temporal interaction architecture. Specifically, we perform unified spatial modeling (introduced in Section 3.1) only once at the beginning of the network, and make the generated spatial features interact with temporal features from different layers. In this way, we can achieve sufficient spatio-temporal interaction without alternately stacking spatial and temporal modeling modules. Meanwhile, considering that the temporal modeling modules at different layers require to interact with different spatial features, we divide the spatial

features S into M groups along the channel dimension, producing spatial sub-features $\{S_i \in \mathbb{R}^{\frac{C^s}{M} \times T \times V} \mid i \in [1, M]\}$, as shown in Fig. 4 (left). To enable the interaction with the temporal features, we further transform the sub-features into $\hat{S}_i \in \mathbb{R}^{T \times V} = \mathcal{R}(S_i)$ to align with the number of dimensions of temporal features, as shown in Fig. 4 (right). \mathcal{R} is the transformation function and we use convolution by default. Finally, different groups of spatial sub-features can express distinct spatial semantics and we let them interact with different layers of temporal modeling to achieve sufficient interaction, as shown in Fig. 3, while avoiding the over-smoothing of spatio-temporal semantics caused by cascaded interaction.

Adaptive interaction. Instead of simple summation, we achieve adaptive spatio-temporal interaction by cross-attention [77]. Given the temporal features $H_{(l)}$ output by the l -th JTM and the spatial sub-features $\hat{S}_{(l+1)}$, the spatio-temporal features $R_{(l)} \in \mathbb{R}^{C^t \times T}$ can be generated as follows:

$$\begin{aligned} R_{(l)} &= \text{DSTI}(\hat{S}_{l+1}, H_{(l)}) \\ &= \text{Softmax} \left(\frac{(W^C \hat{S}_{l+1}) H_{(l)}^T}{\tau} \right) H_{(l)} + H_{(l)}, \end{aligned} \quad (3)$$

where W^C is a 1D convolution that adjusts the dimension of the \hat{S}_{l+1} to match that of $H_{(l)}$, and τ is the temperature parameter controlling the sharpness of the attention maps. This flexible interaction enables our DeST to capture rich spatio-temporal features.

Discussion. Some methods [46], [59], [78] also divide features within a layer and capture multi-scale features by hierarchical connections. Unlike them, our DeST divides distinct spatial sub-features to adaptively interact with temporal features from different layers and aims at decoupling cascaded spatio-temporal interaction. Experiments also show that the divided spatial sub-features can adapt to different actions and enable adaptive spatio-temporal interaction. Please refer to Section 4.5 for more details. Meanwhile, compared to the multi-stream fusion methods [10], [60], [70], [71] that decompose the spatial and temporal information into multiple separate branches, DeST utilizes a single stream to capture spatio-temporal dependencies under a unified spatio-temporal domain.

3.3 Joint-decoupled Temporal Modeling

It is critical to capture rich temporal dependencies of joints in long skeleton sequences. Recent action segmentation methods [20], [21] perform temporal modeling over joints using 2D temporal convolutions. Among these approaches, a major problem is that they usually capture temporal information of each joint by joint-shared weights, eliminating the differences in motion speed between joints and limiting the temporal representations of motion. On the contrast, we propose a Joint-decoupled Temporal Modeling (JTM) module that decouples the temporal modeling of different joints, *i.e.*, the temporal dependencies of each joint are captured by an independent weight, as shown in Fig. 5. In this way, the model can capture temporal dependencies that represent the distinct motion patterns of each joint and generate rich temporal semantics.

Temporal modeling by independent weights. To model the temporal dependencies of different joints separately, we employ independent joint-decoupled weights to perform the convolution operation with each joint, as shown in Fig. 5. The input of the

1. The normalized matrix can be represented as $\hat{A}^{(k)} = D^{-\frac{1}{2}} A^{(k)} D^{\frac{1}{2}}$, where $D_i = \sum_j A_{ij} + \beta$ is a degree matrix and β is set to 0.001.

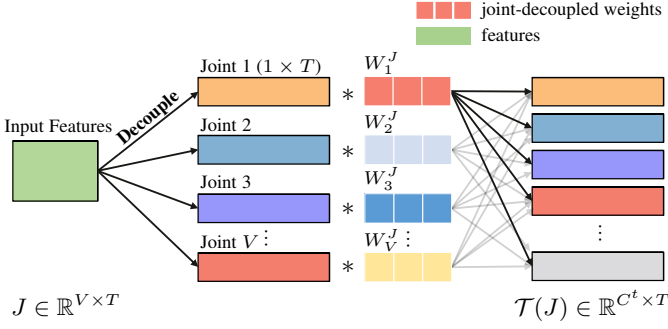


Fig. 5. The process of Joint-decoupled Temporal Modeling (JTM), where V , T , and C^t denote the numbers of input channels, frames, and output channels, respectively. $*$ represents the convolution operation.

JTM can be spatial sub-features or spatio-temporal features generated by the spatio-temporal interaction (DSTI) layers. Without loss of generality, we represent the input as $J \in \mathbb{R}^{V \times T}$. Taking the v -th $J_v \in \mathbb{R}^{1 \times T}$ as an example, an independent convolution with kernel size C^f and weights $W_v^J \in \mathbb{R}^{C^t \times C^f}$ is used to model its temporal dependencies $W_v^J * J_v$. Here, C^t is the number of channels and $*$ denotes the convolution operation. Furthermore, by fusing the temporal dependencies of all joints, the high-level temporal features, *i.e.*, $\mathcal{T}(J) \in \mathbb{R}^{C^t \times T}$, can be generated as follows:

$$\mathcal{T}(J) = \sum_{v=1}^V (W_v^J * J_v). \quad (4)$$

In such decoupled joint modeling, the convolution weights utilized by each joint are independent and do not interfere with each other. Thus, it can learn the distinct motion attributes of different joints and enhance the temporal semantic representations. The joint-decoupled modeling is a general temporal modeling strategy for long skeleton sequences. In the following, we extend the JTM module by the dilated residual TCNs [34] and the linear transformer [79].

Temporal modeling with dilated residual TCNs. Following the previous approaches [34], [42], we employ dilated residual TCNs as $\mathcal{T}(\cdot)$ to capture the temporal features. Specifically, the computation of TCNs can be formally described as follows:

$$\mathcal{T}(J) = \sum_{v=1}^V \text{DConv}(W_v^J, J_v) + J_v, \quad (5)$$

where $\text{DConv}(W_v^J, J_v)$ denotes the dilated convolutional operation with weights W_v^J and input J_v . By stacking multiple layers of JTM, both the short-distance and long-distance temporal relationships between joints can be captured.

Temporal modeling with linear transformer. Unlike TCNs that capture features under a fixed temporal receptive field, the linear transformer [79] can be applied as $\mathcal{T}(\cdot)$ to model the global temporal dependencies of joints. Formally, the linear transformer layer can be computed as follows:

$$\mathcal{T}(J) = \sum_{v=1}^V \phi(Q_v)(\phi(F_v)^T U_v) + J_v, \quad (6)$$

where Q_v , F_v , and U_v are transformed from J_v by the linear layers, and $\phi(\cdot)$ is the activation function. Compared to the previous methods [38] that use sliding window attention, the linear transformer is more suitable for modeling long sequences due to its linear complexity.

3.4 Decoupled spatio-temporal Framework

Overall architecture. By combining the DSTI and JTM modules, we construct a powerful spatio-temporal framework, *i.e.*, DeST, for skeleton-based action segmentation. The full architecture of the proposed DeST is shown in Fig. 3. Specifically, the spatial features generated by unified spatial modeling are divided into M groups of spatial sub-features. Then, L_y layers of Joint-decoupled Temporal Modeling (JTM) are used to capture the rich temporal relationships among joints. The first layer of JTM takes the first spatial sub-feature \hat{S}_1 as input, capturing the temporal dependencies of each joint. In the next $L_y - 1$ JTM layers, such as the l -th layer JTM, the input is the spatio-temporal features R_{l-1} , which are generated from the decoupled spatio-temporal interaction involving spatial sub-features of the l -th group and the temporal features from $(l - 1)$ -th layer of JTM. Overall, the above process can be summarized as follows:

$$H_{(l)} = \begin{cases} \mathcal{T}(\hat{S}_1), & \text{if } l = 1, \\ \mathcal{T}(R_{l-1}), & \text{if } 1 < l \leq L_y, \end{cases} \quad (7)$$

where $H_{(l)}$ is the output features of the l -th layer in DeST. Then, we attain the spatio-temporal features $H_{(L_y)}$ from the last layer. To predict the probability for the action category and action boundary of each frame, we apply two 1D convolutions over the spatio-temporal features $H_{(L_y)}$ as follows:

$$Y_c = \text{Softmax}(\text{Conv1D}(H_{(L_y)})), \quad (8)$$

$$Y_b = \text{Sigmoid}(\text{Conv1D}(H_{(L_y)})), \quad (9)$$

where $Y_c \in R^{C^o \times T}$ denotes the probabilities of the action category, C^o is the total number of action categories, and $Y_b \in R^{1 \times T}$ represents the probability that a frame is at the edge of the action. Following ASRF [38], [42], to improve the performance of action segmentation, we further refine the initial predictions Y_c and Y_b via action segmentation branch (ASB) and boundary regression branch (BRB), respectively. In DeST, the ASB and BRB branches utilize two and three stages of temporal modeling stages [38], [42], respectively.

TABLE 2
The statistics of action segmentation datasets. Seq# denotes the number of frames in an untrimmed long video.

Dataset	videos#	class#	clip#	Seq#	FPS
MCFS-22	271	22	12	~6000	30
MCFS-130	271	130	12	~6000	30
PKU-MMD	1009	42	7	~1000	30
LARa	377	8	22	~6000	50

Loss function. We use cross entropy for the action segmentation branch as the classification loss \mathcal{L}_{ce} following existing works [34], [42]. To penalize over-segmentation errors, the Gaussian similarity-weighted TMSE loss $\mathcal{L}_{gs-tmse}$ [42] is used to smooth the transition of class probabilities between frames. Overall, the loss function for predictions at each stage in the action segmentation branch is defined as follows:

$$\mathcal{L}_{asb} = \mathcal{L}_{ce} + \mathcal{L}_{gs-tmse}. \quad (10)$$

For the boundary regression branch, we use a binary logistic regression loss \mathcal{L}_{brb} at each stage as follows:

$$\mathcal{L}_{brb} = \frac{1}{T} \sum_{t=1}^T (w_p P_b(t) \cdot \log Y_b(t) + (1 - P_b(t)) \cdot \log (1 - Y_b(t))), \quad (11)$$

TABLE 3

Comparison with the state-of-the-art on MCFS-22 [26] and MCFS-130 datasets [26]. † represents that the model uses TCNs instead of the linear transformer in the joint-wise temporal modeling (JTM). * indicates the model has an additional TSR [23] branch.

Methods	FLOPs ↓	Param. ↓	MCFS-130					MCFS-22					
			F1@10 ↑	F1@25 ↑	F1@50 ↑	Edit ↑	Acc ↑	F1@10 ↑	F1@25 ↑	F1@50 ↑	Edit ↑	Acc ↑	
Temporal	MS-TCN [34]	4.04 G	0.67 M	56.4	52.2	42.5	54.5	65.7	74.3	69.7	59.5	74.2	75.6
	SSTDA [80]	-	-	63.8	60.1	49.8	63.5	65.4	76.7	72.2	61.2	77.5	75.7
	ETSPNet [33]	4.41 G	0.74 M	60.9	56.6	47.5	59.8	65.6	74.3	69.9	59.4	73.8	76.6
	ETSN [33]	4.41 G	0.74 M	64.5	61.0	52.3	64.6	64.6	81.4	77.6	66.8	79.8	77.0
	BCN [41]	8.95 G	1.49 M	60.4	55.9	46.4	58.8	68.1	83.4	79.1	67.4	83.7	78.5
	ASRF [42]	7.04 G	1.17 M	66.7	62.3	51.9	65.6	65.6	83.3	80.1	69.2	77.3	75.5
	ASFormer [38]	6.05 G	1.06 M	68.3	64.0	55.1	69.1	67.5	82.8	77.9	66.9	82.3	78.7
Spatio-temporal	MS-GCN [20]	39.97 G	1.10 M	52.4	48.8	39.1	52.6	64.9	75.7	70.5	57.9	72.6	75.5
	SFA+MS-TCN [22]	-	-	-	-	-	-	-	81.3	77.4	67.0	80.0	80.7
	SFA+ETSPNet [22]	-	-	-	-	-	-	-	82.1	78.3	68.6	80.8	81.4
	ID-GCN+ASRF [23]	8.24 G	1.27 M	68.7	65.6	56.9	68.2	67.1	86.4	83.4	73.0	81.6	78.1
	IDT-GCN* [23]	12.81 G	2.03 M	70.7	67.3	58.6	70.2	68.6	88.0	84.9	74.9	84.5	79.9
	DeST† (Ours)	4.91 G	0.76 M	74.0	70.7	61.8	73.8	70.5	86.6	83.5	73.2	82.3	78.7
	DeST (Ours)	6.89 G	1.10 M	75.8	72.2	63.0	75.8	71.4	87.4	84.5	75.0	85.2	80.4
DeST* (Ours)	12.32 G	2.00 M	79.0	75.4	66.0	78.4	73.1	88.1	85.4	76.2	84.9	80.5	

where $P_b(t)$ is the ground truth that only encodes the value of 1 at the action boundary. w_p is the weight of positive samples (*i.e.*, the reciprocal of the number of boundaries over the whole frames), which balances the weights of the number of boundary frames and other frames. In summary, the action segmentation branch and boundary regression branch can be jointly trained with the loss function as follows:

$$\mathcal{L} = \mathcal{L}_{\text{asb}} + \gamma \mathcal{L}_{\text{brb}}, \quad (12)$$

where γ is the loss weight that is set to 0.1 by default.

4 EXPERIMENTS

4.1 Datasets

We evaluate the proposed DeST for skeleton-based action segmentation on four datasets, including MCFS-22 [26], MCFS-130 [26], PKU-MMD [27], and LARa [28]. The statistics of these datasets are listed in Tab. 2.

MCFS-22. The MCFS-22 is a high-quality action segmentation dataset containing 271 long sequences of the skeleton action. Each long video consists of an average of 12 action segments, with an average duration of 212 seconds. The action segments are categorized into 22 classes. Each skeleton graph contains $V = 25$ body joints extracted by the OpenPose toolbox [81].

MCFS-130. Compared to the MCFS-22, the MCFS-130 involves more fine-grained actions in both spatial and temporal dimensions and contains 130 action categories.

PKU-MMD. The PKU-MMD is a large-scale dataset focusing on long continuous sequences for human action understanding. It contains 42 action categories and 1009 long MoCap sequences recorded in three camera views. MoCap sequences are recorded as the 3-axis locations of 25 body joints via the Kinect V2 sensor. This dataset contains two benchmarks: (1) X-sub (X-sub) where training data comes from 775 videos and testing data comes from the other 234 videos. (2) X-view (X-view) where training data comes from the middle and right camera views and testing data comes from the left camera view.

LARa. The LARa is a continuous action dataset where 14 subjects carry out typical warehousing activities. It contains 377 long videos covering 8 action categories. The actions were performed

under 3 different real-world warehousing scenarios. Following the settings of previous works [20], we down-sample the sampling frequency of action sequences from 200 fps to 50 fps.

4.2 Evaluation Metrics

Following previous works, we report three evaluation metrics, *i.e.*, frame-wise accuracy (Acc), segmental edit score, and segmental F1 score at the intersection over union thresholds 0.10, 0.25, and 0.5 (F1@10, F1@25, F1@50). For MCFS-22 and MCFS-130 datasets, the 5-fold cross-validation is used for evaluation, and the averaged results are reported as shown in Tab. 3. For PKU-MMD (X-sub), PKU-MMD (X-view), and LARa datasets, the single validation is used for evaluation, and the results are reported as shown in Tab. 4, Tab. 5, and Tab. 6.

4.3 Implementation Details

All experiments are conducted on a single RTX 3090 GPU with the PyTorch [82], [83] deep learning framework. By default, DSTF adopts the linear transformer [79] for temporal modeling in JTM. The hyper-parameters M and L_c defined in Section 3.4 are set to 10 and 10, respectively, and are discussed in ablation studies (Section 4.7). We use an Adam optimizer for training on all datasets and keep all other hyper-parameters the same as [42]. For MCFS-22 and MCFS-130, we train the models for 300 epochs with a learning rate of 0.0005, a batch size of 1, and the data pre-processing in [26]. For the PKU-MMD and LARa datasets, we train the models for 150 epochs, where the learning rate is 0.001, the batch size is 8, and the data pre-processing follows [20]. In the ablation study, all experiments use the above settings for a fair comparison.

4.4 Comparison with the State-of-the-Art

We compare the proposed DeST with existing state-of-the-art methods, including temporal modeling methods [34], [38], [41], [42], [80] and spatio-temporal modeling methods [20], [22], [23], on the MCFS-22, MCFS-130, PKU-MMD (X-sub), PKU-MMD (X-view), and LARa datasets, respectively.

Comparison with Temporal Modeling Methods. We first compare DeST against temporal modeling methods, including TCN-based methods (*e.g.*, ASRF [42], BCN [41], and MS-TCN

TABLE 4

Comparison with the state-of-the-art on the PKU-MMD dataset using the benchmark of x-sub.

Methods	F1@10 \uparrow	F1@25 \uparrow	F1@50 \uparrow	Edit \uparrow	Acc \uparrow
Online-LSTM [84]	-	-	23.3	-	57.7
TCN [32]	-	-	13.8	-	61.9
ST-GCN [61]	-	-	15.5	-	64.9
MS-TCN [34]	-	-	46.3	-	65.5
MS-GCN [20]	-	-	51.6	-	68.5
CTC [21]	69.9	66.4	53.8	-	69.2
DeST [†] (Ours)	71.7	68.0	55.5	66.3	67.6
DeST (Ours)	74.5	71.0	58.7	69.3	70.3

TABLE 5

Comparison with the state-of-the-art on the PKU-MMD dataset using the benchmark of x-view. ([‡] indicates our implemented results).

Methods	F1@10 \uparrow	F1@25 \uparrow	F1@50 \uparrow	Edit \uparrow	Acc \uparrow
MS-TCN [34] [‡]	58.6	53.6	39.4	56.6	58.2
ETSN [33] [‡]	62.4	57.9	44.3	57.6	60.7
ASRF [42] [‡]	62.5	58.0	46.1	59.3	60.4
MS-GCN [20] [‡]	61.3	56.7	44.1	58.1	65.3
DeST [†] (Ours)	63.2	59.2	47.6	58.2	62.4
DeST (Ours)	69.3	65.6	52.0	64.7	67.3

TABLE 6

Comparison with the state-of-the-art on the LARa dataset.

Methods	F1@10 \uparrow	F1@25 \uparrow	F1@50 \uparrow	Edit \uparrow	Acc \uparrow
Bi-LSTM [85]	-	-	32.3	-	63.9
TCN [32]	-	-	20.0	-	61.5
ST-GCN [61]	-	-	25.8	-	67.9
MS-TCN [34]	-	-	39.6	-	65.8
MS-TCN++ [35]	-	-	40.1	52.3	63.4
BCN [41]	-	-	48.2	57.3	65.4
ASRF [42]	-	-	50.2	60.3	69.5
MS-GCN [20]	-	-	43.6	-	65.6
STGA-Net [48]	-	-	53.3	65.4	70.4
DeST [†] (Ours)	69.7	66.7	55.8	63.7	72.6
DeST (Ours)	70.3	68.0	57.7	64.2	75.1

[34]) and Transformer-based methods (e.g., ASFormer [38]). Compared to the proposed DeST, these methods cannot model spatial information of joints that is essential for skeleton-based action segmentation, thus limiting their performance. As shown in Tab. 3, DeST consistently outperforms these methods. For example, on MCFS-130 in terms of F1@50, DeST that employs TCNs [34] in temporal modeling outperforms the TCN-based ASRF by 7.3%. DeST that employs the linear transformer [79] in temporal modeling also outperforms the Transformer-based ASFormer by 7.5%.

Comparison with spatio-temporal Modeling Methods. Here, we compare our method with the approaches based on spatio-temporal modeling. Even though these methods have implemented spatial modeling, DeST still outperforms previous competitive methods on MCFS-22 and MCFS-130, as shown in Tab. 3. For example, on the challenging MCFS-130 dataset, DeST outperforms the previous SOTA method IDT-GCN by 5.1% in terms of F1@10 with less computational complexity. On MCFS-22, DeST also achieves a significant advantage in single-frame accuracy and segmental edit distance scores compared to IDT-GCN, while performing similar F1 scores with IDT-GCN. This is because IDT-GCN employs an additional Temporal Segment Regression (TSR) branch that models action sequences

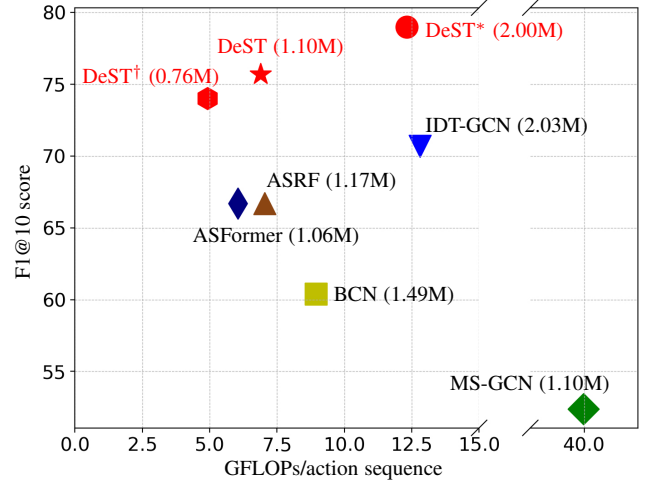


Fig. 6. The F1@10 score and GFLOPs of different methods on the MCFS-130 dataset. The values in the brackets indicate the number of parameters. The proposed DeST outperforms previous methods in terms of segmentation quality, parameter amounts, and GFLOPs.

for recognizing similar frames but requires more computational resources. We also add the TSR branch to DeST, *i.e.*, DeST* in Tab. 3, which results in state-of-the-art performance on both MCFS-22 and MCFS-130.

To further explore the effectiveness of our DeST, we show the comparison on more datasets, including PKU-MMD and LARa. As shown in Tab. 4, Tab. 5, and Tab. 6, we can observe that DeST consistently achieves the best performance, especially on F1 scores. These results demonstrate that DeST predicts more precise and complete action segments across different scenes.

Efficiency analysis. To validate the efficiency, we compare the proposed DeST with existing methods in terms of the number of parameters and GFLOPs. As shown in Fig. 6, our method achieves state-of-the-art performance without sacrificing computational efficiency. In particular, DeST[†] is superior to the previous methods and is lightweight on FLOPs and the number of parameters (e.g., $2.5 \times$ less FLOPs than IDT-GCN and $8.0 \times$ less FLOPs than MS-GCN). DeST and DeST* further achieve higher performances with less computation costs than the previous state-of-the-art methods.

Qualitative results. We further provide qualitative analysis. As shown in Fig. 7, the previous action segmentation methods fail to accurately locate the actions in the long sequence. Especially, the fine-grained actions in MCFS-130 share similar appearance and motion patterns, leading some methods to produce incorrect predictions. For example, as shown in Fig. 7(a), BCN and ETSN produce over-segmentation errors, *i.e.*, segmenting a complete action clip into different categories. ASRF also falsely detects the action boundaries, and IDT-GCN loses some action segments, as shown in Fig. 7(b). MS-GCN also generates a lot of over-segmentation errors, as shown in Fig. 7(c) and (d). These incorrect predictions limit the application of previous methods in practical applications. In contrast, the proposed DeST effectively captures discriminating spatio-temporal features by decoupling cascaded interaction and joint-decoupled temporal modeling, thus relieving these incorrect predictions and achieving better segmentation results. All the above competitive performances and good segmentation results verify the effectiveness of the DeST.

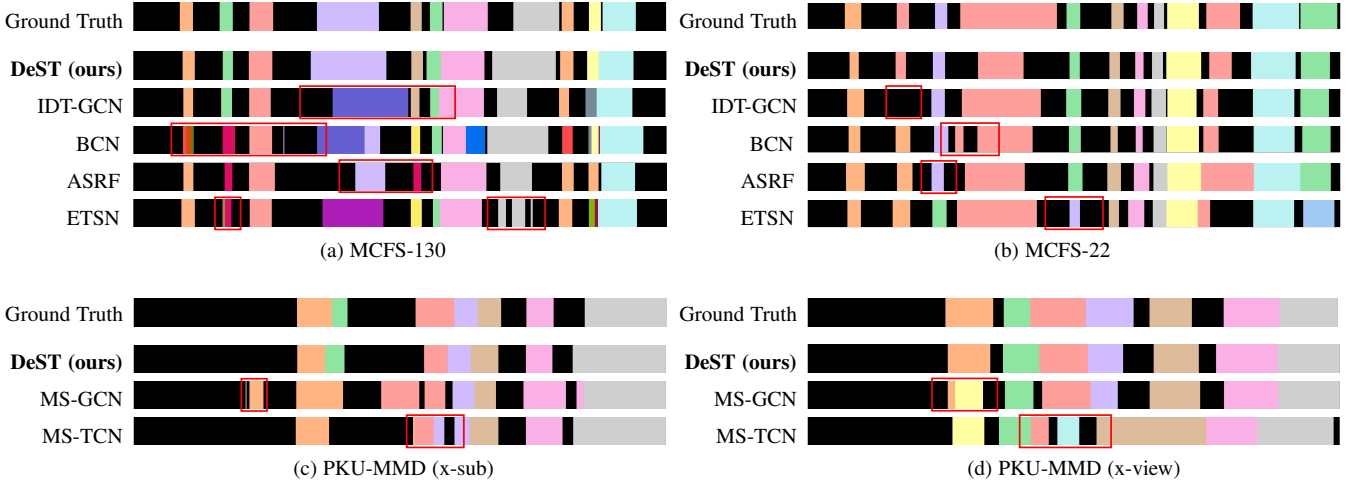


Fig. 7. The qualitative results of action segmentation on MCFS-130, MCFS-22, and PKU-MMD datasets. The segmentation visualization is in the temporal order of actions (from left to right). The different colors represent different action categories. The red box indicates that the models wrongly detect some actions or produce many over-segmentation errors.

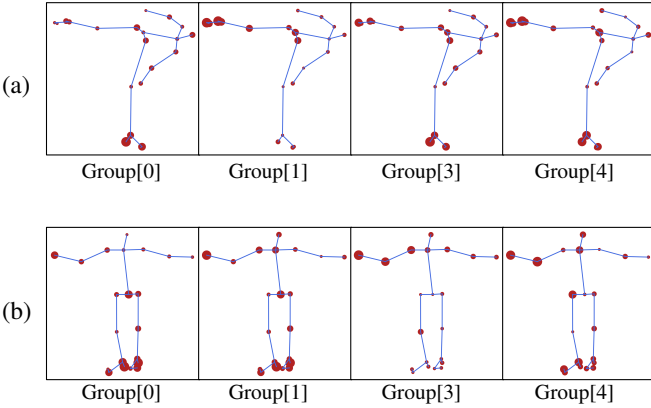


Fig. 8. The activation values (proportional to the size of the red dot) of different groups of spatial sub-features. The larger the red dot is, the corresponding joint play a more important role in spatio-temporal modeling. (a) and (b) show the sub-features in two different actions, *i.e.*, Toeloop_Toeloop and StepSequence, respectively.

4.5 Analysis of Decoupled spatio-temporal Interaction

Effects of spatial sub-features. The sub-features introduced in Section 3.2 contain diverse spatial information and are used to interact with the temporal features from different layers. To analyze the diversity, we first visualize the activation values of different body joints. As shown in Fig. 8, different groups of sub-features focus on different joints. For example, in action (a), the first two groups focus on the bottom *foot*, and the last two groups focus on the top *foot*. Meanwhile, Fig. 8 also shows that the spatial sub-features can adapt to different actions. For instance, the same group pays more attention to the *foot* and *leg* for action (a) but focuses more on the *foot* and *hand* for action (b). This phenomenon indicates that different groups of spatial sub-features can capture diverse and discriminative spatial features, effectively facilitating the spatio-temporal interaction.

Different types of spatio-temporal interaction. To verify the effectiveness of the proposed DSTI module, we compare different interaction methods, including the choice of spatial features and the way of spatio-temporal interaction. As shown in Tab. 7, 1) Compared to the same spatial features interacting with temporal features from different layers, employing spatial sub-features sig-

TABLE 7
Comparison of various spatio-temporal interaction approaches on the MCFS-130 dataset (split #1). SSF (✓) denotes that spatial sub-features are employed. The summation and cross-attention are different interaction manners in the proposed decoupled spatio-temporal interaction (STI).

SSF	STI	F1@10 ↑	F1@25 ↑	F1@50 ↑	Edit ↑	Acc ↑
✗	summation	69.3	65.9	56.8	68.9	68.6
✓	summation	72.5	69.0	60.4	71.5	69.0
✗	cross-attention	73.2	69.0	59.5	71.8	69.5
✓	cross-attention	74.3	71.5	61.9	73.7	69.9

(a) Adopting TCN in joint-decoupled temporal modeling.

SSF	STI	F1@10 ↑	F1@25 ↑	F1@50 ↑	Edit ↑	Acc ↑
✗	summation	72.6	69.3	60.2	73.3	69.9
✓	summation	73.1	69.8	60.8	72.1	69.2
✗	cross-attention	74.2	70.1	61.7	74.3	69.9
✓	cross-attention	76.1	71.8	62.1	76.3	70.6

(b) Adopting transformer in joint-decoupled temporal modeling.

nificantly improves the performance. This phenomenon indicates that the temporal features from different layers require to interact with distinct spatial features, which can be provided by our spatial sub-features. 2) Regarding the interaction scheme, cross-attention outperforms summation, demonstrating the advantage of adaptive interaction. 3) Through combining the spatial sub-features and cross-attention, *i.e.*, our proposed decoupled spatio-temporal interaction architecture, we can achieve the best performance.

Qualitative comparison. Other than the above quantitative analysis, we provide qualitative results for a more comprehensive analysis. Firstly, we utilize t-SNE [86] to show the embedding distribution of different layers generated by MS-GCN [20] and our approach. As shown in Fig. 9(a), we find that along with the increase of MS-GCN layers, the representations between different categories tend to be consistent, especially making action boundaries ambiguous. This shows that as the number of spatio-temporal blocks increases, the problem of over-smoothing is more likely to occur in the methods based on cascaded interaction. In contrast, through decoupling the cascaded interaction, our proposed DeST alleviates the problem of over-smoothing features

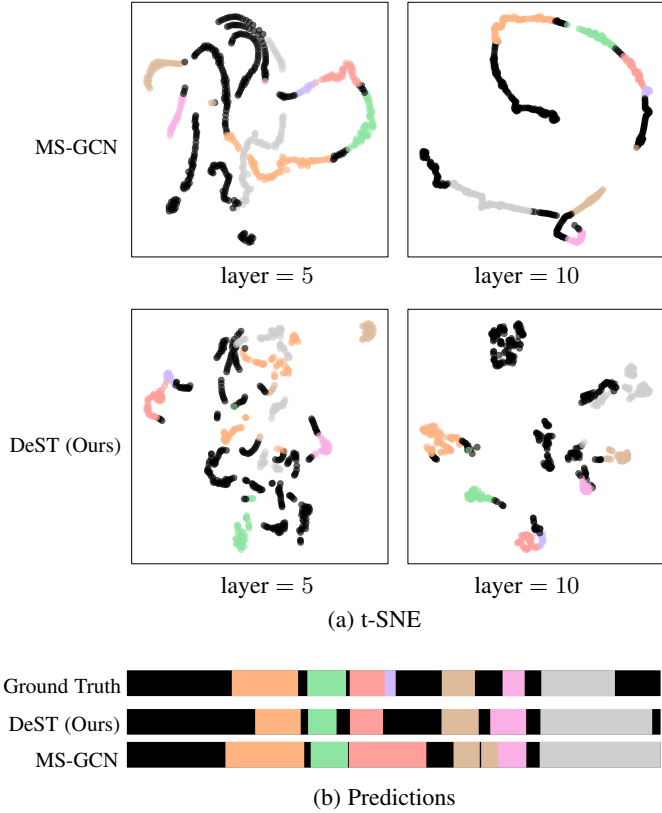


Fig. 9. The (a) t-SNE visualization and (b) corresponding predictions from different layers of MS-GCN [20] and the proposed DeST. In (a), the features output by the temporal modeling layer are visualized and different colors indicate the different categories in the PKU-MMD (x-sub). In (b), the three rows show the ground-truth labels, the predictions from DeST, and the predictions from MS-GCN.

and achieves more separable category boundaries. Specifically, with the increase of network layers, the features from the same category are gradually pulled together, and the features from different categories are pushed away, indicating that our model could capture more discriminative spatio-temporal relations. This phenomenon is also demonstrated in Section 4.7, where we show that using more layers of spatio-temporal interaction (DSTI) leads to better performances. Meanwhile, the predictions corresponding to the features of Fig. 9(a) also verify that our model can segment action boundaries accurately, as shown in Fig. 9(b).

4.6 Analysis of Joint-decoupled Temporal Modeling

Statistics on the motion speed of joints. To verify the motivation of the joint-decoupled temporal modeling, we count the movement speed of different joints in all sequences from MCFS-130. As shown in Fig. 10, different joints move at different speeds. For example, compared to the joints near the spine, the joints in the shoulders and legs move faster and have a high variance in speed. This phenomenon supports our motivation to model different joints separately.

Comparison of joint-decoupled/shared weights. To compare the effect of independent or shared weights for modeling temporal information, we compare the previous temporal convolution networks [20] that utilize dilated 2D convolution (kernel size is 1×3), denoted as 2D-Conv, to model all joints in shared weights way and our proposed JTM. To focus on the temporal modeling capabilities of the model, we employ the baseline that

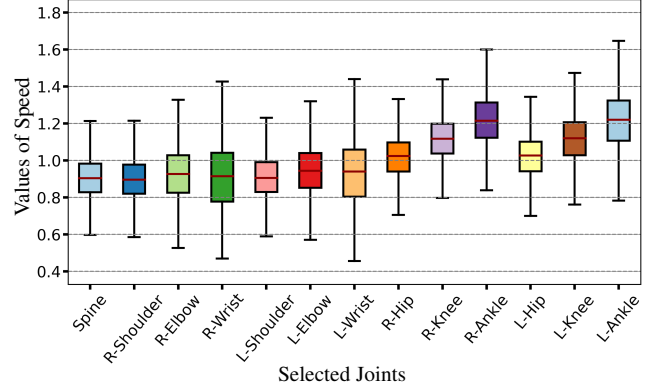


Fig. 10. Motion speeds of different joints. We count the speeds of joint by all samples in the MCFS-130 dataset. Different boxes represent the speed range of different joints: 1) the red line inside each box denotes the median value; 2) boxes boundaries means the first quartile and the third quartile of the data, respectively; 3) upper and lower whiskers indicate the max value and min value, respectively.

TABLE 8

Comparison of joint-decoupled and joint-shared weights. JWTM defined by Section 4.6 means the module that uses shared weights to model all joints.

Model		F1@10 ↑	F1@25 ↑	F1@50 ↑	Edit ↑	Acc ↑
TCN	2D-Conv	85.3	81.6	70.8	80.9	78.1
	JWTM	85.7	82.0	71.1	81.6	77.4
	JTM	87.2	83.6	72.8	82.6	78.1
Transformer	JWTM	80.6	75.9	65.6	78.7	75.3
	JTM	86.7	83.6	73.9	83.7	79.1

(a) Comparison on the MCFS-22 dataset (split #1).

Model		F1@10 ↑	F1@25 ↑	F1@50 ↑	Edit ↑	Acc ↑
TCN	2D-Conv	68.8	65.3	56.1	67.0	67.0
	JWTM	69.4	65.8	57.1	68.6	67.9
	JTM	71.2	67.5	59.1	70.6	68.8
Transformer	JWTM	71.4	66.5	58.0	71.6	68.1
	JTM	72.5	69.4	59.7	73.0	69.4

(b) Comparison on the MCFS-130 dataset (split #1).

only performs a single spatio-temporal interaction [22], [23]. As shown in Tab. 8, using TCN for timing modeling, the models with the JTM module achieve better performance than the models with 2D-Conv for all metrics in both MCFS-22 and MCFS-130. For example, our JTM module can improve the 2D-Conv at 3.0% on the F1@50 score on MCFS-130.

The above comparison is only conducted by utilizing TCN as temporal modeling. To further explore the validity of JTM, we conduct a Joint-shared Weight Temporal Modeling (JWTM) module that employs the dilated residual TCNs [34] and the linear transformer [79] and compare the JWTM with the proposed JTM. For the implementation of JWTM, the input features $S' \in \mathbb{R}^{C' \times T \times V}$ are transformed into channel-level features $\hat{S}' \in \mathbb{R}^{C' \times T}$ via the \mathcal{R} function. Different from Eq. 4, the output features $\mathcal{T}(\hat{S}') \in \mathbb{R}^{C' \times T}$ of the JWTM are represented as:

$$\mathcal{T}(\hat{S}') = \sum_{c=1}^{C'} (W_c^J * \hat{S}'_c). \quad (13)$$

The temporal features generated by JWTM ignore the differences in the motion of different joints. Unlike JTM which models each

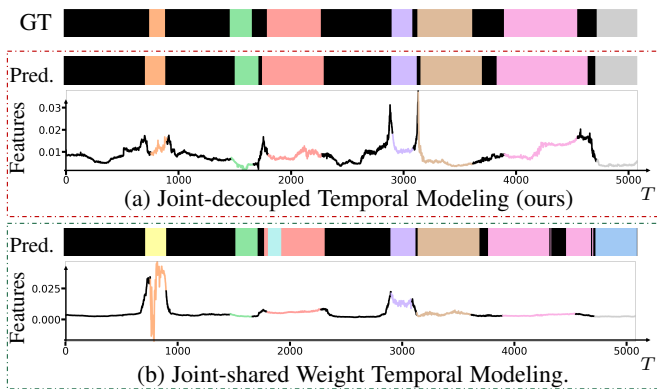


Fig. 11. The visualization of predictions and temporal features output by JTM and JWTM. We take a sequence from the MCFS-22 dataset as an example. The dimension of the temporal feature is $C^t \times V$, and the horizontal axis represents the temporal order of actions (from left to right). About visualization, we average the temporal features along channels, and different colors represent different categories of action.

TABLE 9
The effect of different feature-transform functions on the MCFS-22 dataset (split #1).

\mathcal{R}	F1@10 \uparrow	F1@25 \uparrow	F1@50 \uparrow	Edit \uparrow	Acc \uparrow
Avg pooling	86.4	82.7	73.2	82.8	78.6
Max pooling	84.6	81.1	71.0	80.9	78.3
Convolution	86.7	83.6	73.9	83.7	79.1

joint by independent weights, JWTM captures temporal dependencies of all joints using shared weights. As shown in Tab. 8, the models with the JTM module output the model with the JWTM. We also observe that the linear transformer using the JWTM results in a huge drop in performance on MCFS-22. This indicates the importance of modeling the motion properties of each joint and the effectiveness of the JTM module in capturing the temporal dependencies of individual joints.

Qualitative analysis. To delve deeper into the difference between JTM and JWTM modules and how they affect the final performance, we visualize the predictions and temporal features extracted from the last layer when using JTM and JWTM, respectively. As shown in Fig. 11, regarding the predictions, we observe that our proposed JTM module identifies each action clip correctly. In contrast, the JWTM module fails to distinguish action boundaries and predicts the wrong action categories. This is because the JWTM ignores differences in motion speed of different joints, thus weakening the temporal modeling semantics. This effect can also be seen from the temporal features, as shown in Fig. 11, where the learned features are too smooth and lack distinction. In contrast, the JTM enables the model to learn distinctive temporal dependencies from each joint, helping identify multiple action clips in long sequences.

4.7 Ablation Analysis

Different feature transformation functions. In Section 3.2, we propose the feature transformation function to align the dimensions between spatial and temporal features. Here, we explore the effects of different feature transformation functions. As shown in Tab. 9, the models with Convolution and Avgpool outperform the models with Maxpool. This is because the Maxpool is susceptible to outliers and may result in the loss of necessary information for identifying action boundaries. In contrast,

TABLE 10
The effect of the number of the JTM layers (L_y) for temporal modeling on MCFS-130 dataset (split #1).

L_y	F1@10 \uparrow	F1@25 \uparrow	F1@50 \uparrow	Edit \uparrow	Acc \uparrow
8	72.0	68.7	58.5	74.0	69.7
9	74.1	70.9	61.6	73.5	70.3
10	76.3	73.1	63.4	76.8	70.5
11	75.2	71.3	61.2	75.5	69.5
12	74.8	72.0	60.8	75.3	69.6

TABLE 11
The effect of the number of the interaction (DSTI) layers (L_c) on MCFS-130 dataset (split #1).

L_c	F1@10 \uparrow	F1@25 \uparrow	F1@50 \uparrow	Edit \uparrow	Acc \uparrow
1	72.6	69.2	60.7	73.1	69.0
2	73.3	70.0	60.9	73.1	69.9
3	74.2	70.6	61.5	73.3	70.4
4	74.3	70.1	62.0	74.4	69.5
5	74.8	71.0	61.1	74.4	70.0
6	74.8	71.0	62.7	74.3	70.4
7	75.1	72.0	62.1	75.0	70.7
8	75.0	71.7	62.8	75.0	70.7
9	76.3	73.1	63.4	76.8	70.5

Avgpool retains overall information about the features, while Convolution processes the features adaptively using trainable weights. Considering the performance of the model, we adopt the Convolution feature-transform function in DeST.

Impact of the number of JTM layers. The number of JTM, *i.e.*, L_y , defines the depth of the temporal modeling network for DeST. As shown in Tab. 10, increasing L_y from 8 to 10 greatly boosts the performance, indicating that enough temporal modeling layers are essential. Adding L_y from 10 to 11 or 12 still improves the performance, but the improvements are less significant than increasing from 8 to 10.

Effect of the number of DSTI layers. We also conduct ablation experiments about the number of DSTI layers, where only the first L_c JTM layers, perform the interaction with spatial features and temporal features. As shown in Tab. 11, the performance is significantly improved when increasing the L_c from 1 to 9. This is mainly because the proposed decoupled interaction will not cause the problem of over-smoothing, thus making the spatio-temporal features more discriminative. To better understand the behavior of the decoupled spatio-temporal interaction layers, we also visualize the cross-attention maps from different layers of DSTI. As shown in Fig. 12, the attention maps vary across various layers. This demonstrates that our adaptive interaction module can learn the different interaction patterns at various layers, which is beneficial for generating distinctive spatio-temporal features.

5 CONCLUSION

In this work, we present a Decoupled Spatio-Temporal Framework (DeST) for skeleton-based action segmentation. Unlike previous spatio-temporal models, DeST adopts decoupled spatio-temporal interaction and joint-decoupled temporal modeling. The decoupled spatio-temporal interaction adopts a single layer of spatial modeling to extract spatial features, which are divided into different groups of spatial sub-features and then interact with temporal features from different layers, avoiding the over-smoothing caused by cascaded interaction. The joint-decoupled temporal modeling decouples the modeling of each joint, enabling the model to capture the distinct motion properties of different

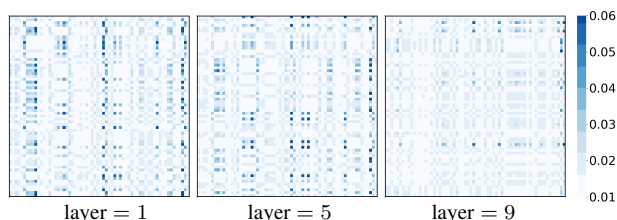


Fig. 12. The visualization of cross-attention weights of different interaction (DSTI) layers.

joints. On four large-scale benchmarks of different scenes, the proposed DeST achieves competitive performance with less computational costs than existing methods. Due to the effectiveness and efficiency, the proposed DeST could serve as a new baseline for spatio-temporal modeling and have a large potential for developing more complex models.

Limitation and Future work. Compared to previous methods, our proposed DeST has significantly improved accuracy in recognizing fine-grained actions, but there are still rooms to improve the performance. In future, we will try fine-grained modeling in the spatial and temporal dimensions to further improve the performance. For example, we can design new spatial topology to model complex spatial relationships of joints effectively and employ multi-stream fusion strategies [72]. Besides, since long action sequences are more accessible than edited action clips, we can also explore self-supervised long-sequence action modeling to get better pre-trained models.

REFERENCES

- [1] X. Luo, H. Li, X. Yang, Y. Yu, and D. Cao, "Capturing and understanding workers' activities in far-field surveillance videos with deep action recognition and bayesian nonparametric learning," *Comput.-aided Civ. Inf.*, vol. 34, no. 4, pp. 333–351, 2019.
- [2] H. Son, H. Choi, H. Seong, and C. Kim, "Detection of construction workers under varying poses and changing background in image sequences via very deep residual networks," *Automat. Constr.*, vol. 99, pp. 27–38, 2019.
- [3] B. Filtjens, A. Nieuwboer, N. D'cruz, J. Spildooren, P. Slaets, and B. Vanrumste, "A data-driven approach for detecting gait events during turning in people with parkinson's disease and freezing of gait," *Gait & Posture*, vol. 80, pp. 130–136, 2020.
- [4] E. Kidziński, S. Delp, and M. Schwartz, "Automatic real-time gait event detection in children using deep neural networks," *PLoS ONE*, vol. 14, no. 1, p. e0211466, 2019.
- [5] J. Kenney, T. Buckley, and O. Brock, "Interactive segmentation for manipulation in unstructured environments," in *ICRA*. IEEE, 2009, pp. 1377–1382.
- [6] M. Siam, C. Jiang, S. Lu, L. Petrich, M. Gamal, M. Elhoseiny, and M. Jagersand, "Video object segmentation using teacher-student adaptation in a human robot interaction (hri) setting," in *ICRA*. IEEE, 2019, pp. 50–56.
- [7] M. Sudha, K. Sriraghav, S. G. Jacob, S. Manisha *et al.*, "Approaches and applications of virtual reality and gesture recognition: A review," *IJCAI*, vol. 8, no. 4, pp. 1–18, 2017.
- [8] A. Biswas, S. Dutta, N. Dey, and A. T. Azar, "A kinect-less augmented reality approach to real-time tag-less virtual trial room simulation," *IJSSMET*, vol. 5, no. 4, pp. 13–28, 2014.
- [9] M. Liu, H. Liu, and C. Chen, "Enhanced skeleton visualization for view invariant human action recognition," *Pattern Recognit.*, vol. 68, pp. 346–362, 2017.
- [10] Y.-F. Song, Z. Zhang, C. Shan, and L. Wang, "Constructing stronger and faster baselines for skeleton-based action recognition," *IEEE Trans. Pattern Anal. Mach. Intell.*, vol. 45, no. 2, pp. 1474–1488, 2022.
- [11] K. Cheng, Y. Zhang, X. He, J. Cheng, and H. Lu, "Extremely lightweight skeleton-based action recognition with shiftgcn++," *IEEE Trans. Image Process.*, vol. 30, pp. 7333–7348, 2021.
- [12] J. Carreira and A. Zisserman, "Quo vadis, action recognition? a new model and the kinetics dataset," in *IEEE Conf. Comput. Vis. Pattern Recog.*, 2017, pp. 6299–6308.
- [13] K. Simonyan and A. Zisserman, "Two-stream convolutional networks for action recognition in videos," *Adv. Neural Inform. Process. Syst.*, vol. 27, 2014.
- [14] L. Wang, W. Li, W. Li, and L. Van Gool, "Appearance-and-relation networks for video classification," in *IEEE Conf. Comput. Vis. Pattern Recog.*, 2018, pp. 1430–1439.
- [15] L. Wang, Y. Qiao, and X. Tang, "Action recognition with trajectory-pooled deep-convolutional descriptors," in *IEEE Conf. Comput. Vis. Pattern Recog.*, 2015, pp. 4305–4314.
- [16] L. Wang, Y. Xiong, Z. Wang, Y. Qiao, D. Lin, X. Tang, and L. Van Gool, "Temporal segment networks: Towards good practices for deep action recognition," in *Eur. Conf. Comput. Vis.*. Springer, 2016, pp. 20–36.
- [17] Z. Liu, J. Ning, Y. Cao, Y. Wei, Z. Zhang, S. Lin, and H. Hu, "Video swin transformer," in *IEEE Conf. Comput. Vis. Pattern Recog.*, 2022, pp. 3202–3211.
- [18] A. Arnab, M. Dehghani, G. Heigold, C. Sun, M. Lučić, and C. Schmid, "Vivit: A video vision transformer," in *Int. Conf. Comput. Vis.*, 2021, pp. 6836–6846.
- [19] L. Wang, B. Huang, Z. Zhao, Z. Tong, Y. He, Y. Wang, Y. Wang, and Y. Qiao, "Videomae v2: Scaling video masked autoencoders with dual masking," in *IEEE Conf. Comput. Vis. Pattern Recog.*, June 2023, pp. 14 549–14 560.
- [20] B. Filtjens, B. Vanrumste, and P. Slaets, "Skeleton-based action segmentation with multi-stage spatial-temporal graph convolutional neural networks," *IEEE Trans. Emerg. Top. Com.*, 2022.
- [21] L. Xu, Q. Wang, X. Lin, and L. Yuan, "An efficient framework for few-shot skeleton-based temporal action segmentation," *Comput. Vis. Image Und.*, vol. 232, p. 103707, 2023.
- [22] K. Liu, Y. Li, Y. Xu, S. Liu, and S. Liu, "Spatial focus attention for fine-grained skeleton-based action tasks," *IEEE Sign. Process. Letters*, vol. 29, pp. 1883–1887, 2022.
- [23] Y.-H. Li, K.-Y. Liu, S.-L. Liu, L. Feng, and H. Qiao, "Involving distinguished temporal graph convolutional networks for skeleton-based temporal action segmentation," *IEEE Trans. Circuit Syst. Video Technol.*, 2023.
- [24] D. Bo, X. Wang, C. Shi, and H. Shen, "Beyond low-frequency information in graph convolutional networks," in *AAAI*. AAAI Press, 2021.
- [25] C. Pang, X. Lu, and L. Lyu, "Skeleton-based action recognition through contrasting two-stream spatial-temporal networks," *IEEE Trans. Multimedia*, 2023.
- [26] S. Liu, A. Zhang, Y. Li, J. Zhou, L. Xu, Z. Dong, and R. Zhang, "Temporal segmentation of fine-grained semantic action: A motion-centered figure skating dataset," in *AAAI*, vol. 35, no. 3, 2021, pp. 2163–2171.
- [27] C. Liu, Y. Hu, Y. Li, S. Song, and J. Liu, "Pku-mmd: A large scale benchmark for skeleton-based human action understanding," in *ACM FASCCW*, 2017, pp. 1–8.
- [28] F. Niemann, C. Reining, F. Moya Rueda, N. R. Nair, J. A. Steffens, G. A. Fink, and M. Ten Hompel, "Lara: Creating a dataset for human activity recognition in logistics using semantic attributes," *Sensors*, vol. 20, no. 15, p. 4083, 2020.
- [29] J. Carreira and A. Zisserman, "Quo vadis, action recognition? a new model and the kinetics dataset," in *IEEE Conf. Comput. Vis. Pattern Recog.*, July 2017.
- [30] L. Ding and C. Xu, "Tricornet: A hybrid temporal convolutional and recurrent network for video action segmentation," *arXiv preprint arXiv:1705.07818*, 2017.
- [31] B. Singh, T. K. Marks, M. Jones, O. Tuzel, and M. Shao, "A multi-stream bi-directional recurrent neural network for fine-grained action detection," in *IEEE Conf. Comput. Vis. Pattern Recog.*, June 2016.
- [32] C. Lea, M. D. Flynn, R. Vidal, A. Reiter, and G. D. Hager, "Temporal convolutional networks for action segmentation and detection," in *IEEE Conf. Comput. Vis. Pattern Recog.*, 2017, pp. 156–165.
- [33] Y. Li, Z. Dong, K. Liu, L. Feng, L. Hu, J. Zhu, L. Xu, S. Liu *et al.*, "Efficient two-step networks for temporal action segmentation," *Neurocomputing*, vol. 454, pp. 373–381, 2021.
- [34] Y. A. Farha and J. Gall, "Ms-tcn: Multi-stage temporal convolutional network for action segmentation," in *IEEE Conf. Comput. Vis. Pattern Recog.*, 2019, pp. 3575–3584.
- [35] S. Li, Y. A. Farha, Y. Liu, M.-M. Cheng, and J. Gall, "Ms-tcn++: Multi-stage temporal convolutional network for action segmentation," *IEEE Trans. Pattern Anal. Mach. Intell.*, vol. 45, no. 6, pp. 6647–6658, 2023.
- [36] S.-H. Gao, Q. Han, Z.-Y. Li, P. Peng, L. Wang, and M.-M. Cheng, "Global2local: Efficient structure search for video action segmentation," in *IEEE Conf. Comput. Vis. Pattern Recog.*, June 2021, pp. 16 805–16 814.
- [37] S. Gao, Z.-Y. Li, Q. Han, M.-M. Cheng, and L. Wang, "Rf-next: Efficient receptive field search for convolutional neural networks," *IEEE Trans. Pattern Anal. Mach. Intell.*, vol. 45, no. 3, pp. 2984–3002, 2022.

- [38] F. Yi, H. Wen, and T. Jiang, "Asformer: Transformer for action segmentation," in *Brit. Mach. Vis. Conf.*, 2021.
- [39] N. Behrmann, S. A. Golestaneh, Z. Kolter, J. Gall, and M. Noroozi, "Unified fully and timestamp supervised temporal action segmentation via sequence to sequence translation," in *Eur. Conf. Comput. Vis.* Springer, 2022, pp. 52–68.
- [40] J. G. Emad Bahrami, Gianpiero Francesca, "How much temporal long-term context is needed for action segmentation?" in *Int. Conf. Comput. Vis.*, 2023.
- [41] Z.-Z. Wang, Z.-T. Gao, L.-M. Wang, Z.-F. Li, and G.-S. Wu, "Boundary-aware cascade networks for temporal action segmentation," in *Eur. Conf. Comput. Vis.* Springer, 2020.
- [42] Y. Ishikawa, S. Kasai, Y. Aoki, and H. Kataoka, "Alleviating over-segmentation errors by detecting action boundaries," in *WACV*, 2021, pp. 2322–2331.
- [43] H. Ahn and D. Lee, "Refining action segmentation with hierarchical video representations," in *Int. Conf. Comput. Vis.*, 2021, pp. 16 302–16 310.
- [44] M. Li, L. Chen, Y. Duan, Z. Hu, J. Feng, J. Zhou, and J. Lu, "Bridge-prompt: Towards ordinal action understanding in instructional videos," in *IEEE Conf. Comput. Vis. Pattern Recog.*, June 2022.
- [45] D. Liu, Q. Li, A.-D. Dinh, T. Jiang, M. Shah, and C. Xu, "Diffusion action segmentation," in *Int. Conf. Comput. Vis.*, 2023.
- [46] Z. Chen, S. Li, B. Yang, Q. Li, and H. Liu, "Multi-scale spatial temporal graph convolutional network for skeleton-based action recognition," in *AAAI*, vol. 35, no. 2, 2021, pp. 1113–1122.
- [47] M. Wang, B. Ni, and X. Yang, "Learning multi-view interactional skeleton graph for action recognition," *IEEE Trans. Pattern Anal. Mach. Intell.*, 2020.
- [48] X. Tian, Y. Jin, Z. Zhang, P. Liu, and X. Tang, "Stga-net: Spatial-temporal graph attention network for skeleton-based temporal action segmentation," in *ICMEW*. IEEE, 2023, pp. 218–223.
- [49] X. Hao, J. Li, Y. Guo, T. Jiang, and M. Yu, "Hypergraph neural network for skeleton-based action recognition," *IEEE Trans. Image Process.*, vol. 30, pp. 2263–2275, 2021.
- [50] S. Li, X. He, W. Song, A. Hao, and H. Qin, "Graph diffusion convolutional network for skeleton based semantic recognition of two-person actions," *IEEE Trans. Pattern Anal. Mach. Intell.*, 2023.
- [51] G. Hu, B. Cui, and S. Yu, "Joint learning in the spatio-temporal and frequency domains for skeleton-based action recognition," *IEEE Trans. Multimedia*, vol. 22, no. 9, pp. 2207–2220, 2019.
- [52] P. Zhang, C. Lan, J. Xing, W. Zeng, J. Xue, and N. Zheng, "View adaptive neural networks for high performance skeleton-based human action recognition," *IEEE Trans. Pattern Anal. Mach. Intell.*, vol. 41, no. 8, pp. 1963–1978, 2019.
- [53] S. Nowozin and J. Shotton, "Action points: A representation for low-latency online human action recognition," *Microsoft Research Cambridge, Tech. Rep.*, 2012.
- [54] A. Sharaf, M. Torki, M. E. Hussein, and M. El-Saban, "Real-time multi-scale action detection from 3d skeleton data," in *WACV*. IEEE, 2015, pp. 998–1005.
- [55] H. Wang and L. Wang, "Beyond joints: Learning representations from primitive geometries for skeleton-based action recognition and detection," *IEEE Trans. Image Process.*, vol. 27, no. 9, pp. 4382–4394, 2018.
- [56] M. Korban and X. Li, "Semantics-enhanced early action detection using dynamic dilated convolution," *Pattern Recognit.*, vol. 140, p. 109595, 2023.
- [57] Q. Cui, H. Sun, and F. Yang, "Learning dynamic relationships for 3d human motion prediction," in *IEEE Conf. Comput. Vis. Pattern Recog.*, 2020, pp. 6519–6527.
- [58] M. Li, S. Chen, Y. Zhao, Y. Zhang, Y. Wang, and Q. Tian, "Dynamic multiscale graph neural networks for 3d skeleton based human motion prediction," in *IEEE Conf. Comput. Vis. Pattern Recog.*, June 2020.
- [59] L. Dang, Y. Nie, C. Long, Q. Zhang, and G. Li, "Msr-gcn: Multi-scale residual graph convolution networks for human motion prediction," in *Int. Conf. Comput. Vis.*, October 2021, pp. 11 467–11 476.
- [60] M. Li, S. Chen, X. Chen, Y. Zhang, Y. Wang, and Q. Tian, "Symbiotic graph neural networks for 3d skeleton-based human action recognition and motion prediction," *IEEE Trans. Pattern Anal. Mach. Intell.*, vol. 44, no. 6, pp. 3316–3333, 2021.
- [61] S. Yan, Y. Xiong, and D. Lin, "Spatial temporal graph convolutional networks for skeleton-based action recognition," in *AAAI*, 2018.
- [62] L. Shi, Y. Zhang, J. Cheng, and H. Lu, "Two-stream adaptive graph convolutional networks for skeleton-based action recognition," in *IEEE Conf. Comput. Vis. Pattern Recog.*, June 2019.
- [63] K. Cheng, Y. Zhang, C. Cao, L. Shi, J. Cheng, and H. Lu, "Decoupling gcn with dropgraph module for skeleton-based action recognition," in *Eur. Conf. Comput. Vis.* Springer, 2020, pp. 536–553.
- [64] Y. Chen, Z. Zhang, C. Yuan, B. Li, Y. Deng, and W. Hu, "Channel-wise topology refinement graph convolution for skeleton-based action recognition," in *Int. Conf. Comput. Vis.*, October 2021, pp. 13 359–13 368.
- [65] Y.-F. Song, Z. Zhang, C. Shan, and L. Wang, "Richly activated graph convolutional network for robust skeleton-based action recognition," *IEEE Trans. Circuit Syst. Video Technol.*, vol. 31, no. 5, pp. 1915–1925, 2020.
- [66] J. Kong, H. Deng, and M. Jiang, "Symmetrical enhanced fusion network for skeleton-based action recognition," *IEEE Trans. Circuit Syst. Video Technol.*, vol. 31, no. 11, pp. 4394–4408, 2021.
- [67] Y. Zhu, H. Shuai, G. Liu, and Q. Liu, "Multilevel spatial-temporal excited graph network for skeleton-based action recognition," *IEEE Trans. Image Process.*, vol. 32, pp. 496–508, 2022.
- [68] J. Liu, X. Wang, C. Wang, Y. Gao, and M. Liu, "Temporal decoupling graph convolutional network for skeleton-based gesture recognition," *IEEE Trans. Multimedia*, 2023.
- [69] B. Xu, X. Shu, J. Zhang, G. Dai, and Y. Song, "Spatiotemporal decouple-and-squeeze contrastive learning for semisupervised skeleton-based action recognition," *IEEE Trans. Neural Networks Learn. Syst.*, 2023.
- [70] E. Aksan, M. Kaufmann, P. Cao, and O. Hilliges, "A spatio-temporal transformer for 3d human motion prediction," in *3DV*. IEEE, 2021, pp. 565–574.
- [71] H. Yu, X. Fan, Y. Hou, W. Pei, H. Ge, X. Yang, D. Zhou, Q. Zhang, and M. Zhang, "Towards realistic 3d human motion prediction with a spatio-temporal cross-transformer approach," *IEEE Trans. Circuit Syst. Video Technol.*, 2023.
- [72] L. Shi, Y. Zhang, J. Cheng, and H. Lu, "Skeleton-based action recognition with multi-stream adaptive graph convolutional networks," *IEEE Trans. Image Process.*, vol. 29, pp. 9532–9545, 2020.
- [73] X. Zhang, C. Xu, X. Tian, and D. Tao, "Graph edge convolutional neural networks for skeleton-based action recognition," *IEEE Trans. Neural Networks Learn. Syst.*, vol. 31, no. 8, pp. 3047–3060, 2019.
- [74] C. Cao, C. Lan, Y. Zhang, W. Zeng, H. Lu, and Y. Zhang, "Skeleton-based action recognition with gated convolutional neural networks," *IEEE Trans. Circuit Syst. Video Technol.*, vol. 29, no. 11, pp. 3247–3257, 2018.
- [75] H. Yang, D. Yan, L. Zhang, Y. Sun, D. Li, and S. J. Maybank, "Feedback graph convolutional network for skeleton-based action recognition," *IEEE Trans. Image Process.*, vol. 31, pp. 164–175, 2021.
- [76] Z. Liu, H. Zhang, Z. Chen, Z. Wang, and W. Ouyang, "Disentangling and unifying graph convolutions for skeleton-based action recognition," in *IEEE Conf. Comput. Vis. Pattern Recog.*, June 2020.
- [77] A. Vaswani, N. Shazeer, N. Parmar, J. Uszkoreit, L. Jones, A. N. Gomez, Ł. Kaiser, and I. Polosukhin, "Attention is all you need," in *Adv. Neural Inform. Process. Syst.*, 2017, pp. 5998–6008.
- [78] S.-H. Gao, M.-M. Cheng, K. Zhao, X.-Y. Zhang, M.-H. Yang, and P. Torr, "Res2net: A new multi-scale backbone architecture," *IEEE Trans. Pattern Anal. Mach. Intell.*, vol. 43, no. 2, pp. 652–662, 2019.
- [79] A. Katharopoulos, A. Vyas, N. Pappas, and F. Fleuret, "Transformers are RNNs: Fast autoregressive transformers with linear attention," in *ICML*, ser. Proceedings of Machine Learning Research, H. D. III and A. Singh, Eds., vol. 119. PMLR, 13–18 Jul 2020, pp. 5156–5165.
- [80] M.-H. Chen, B. Li, Y. Bao, G. AlRegib, and Z. Kira, "Action segmentation with joint self-supervised temporal domain adaptation," in *IEEE Conf. Comput. Vis. Pattern Recog.*, June 2020.
- [81] Z. Cao, T. Simon, S.-E. Wei, and Y. Sheikh, "Realtime multi-person 2d pose estimation using part affinity fields," in *IEEE Conf. Comput. Vis. Pattern Recog.*, July 2017.
- [82] A. Paszke, S. Gross, S. Chintala, G. Chanan, E. Yang, Z. DeVito, Z. Lin, A. Desmaison, L. Antiga, and A. Lerer, "Automatic differentiation in pytorch," *NeurIPS*, 2017.
- [83] A. Paszke, S. Gross, F. Massa, A. Lerer, J. Bradbury, G. Chanan, T. Killeen, Z. Lin, N. Gimelshein, L. Antiga et al., "Pytorch: An imperative style, high-performance deep learning library," *Adv. Neural Inform. Process. Syst.*, vol. 32, 2019.
- [84] F. Carrara, P. Elias, J. Sedmidubsky, and P. Zezula, "Lstm-based real-time action detection and prediction in human motion streams," *Multimed. Tools Appl.*, vol. 78, pp. 27 309–27 331, 2019.
- [85] A. Graves and J. Schmidhuber, "Framewise phoneme classification with bidirectional lstm and other neural network architectures," *Neural networks*, vol. 18, no. 5-6, pp. 602–610, 2005.
- [86] L. Van der Maaten and G. Hinton, "Visualizing data using t-sne." *J. Mach. Learn. Res.*, vol. 9, no. 11, 2008.